

INVESTIGATION OF TRANSIENT AND STEADY HEAT TRANSFER IN SATURATED POROUS MEDIUM FILLED IN A VERTICAL CYLINDER WITH THERMAL DISPERSION AND RADIATION

by

Nabeel ABU SHABAN**, *Ahmad MANASRAH*, and *Ibraheem NASSER

Mechanical Engineering Department, Al-Zaytoonah University of Jordan, Amman, Jordan

Original scientific paper
<https://doi.org/10.2298/TSCI210501344A>

In this study, the influence of thermal radiation and dispersion on a porous medium which was filled in a vertical cylinder was numerically solved. A finite-difference method was used to solve the non-dimensional equations by applying a Crank-Nicolson implicit numerical technique. Moreover, an experimental set-up has been initially built to investigate the effect of three different grain sizes of the porous materials on the heat transfer process. The numerical results indicated that the thermal radiation increased the momentum and the thickness of the thermal boundary-layer during the natural-convection heat transfer process. Whereas, the thermal dispersion factor decreased the momentum and the thickness of the boundary-layer during the natural-convection heat transfer process, which enabled a steady and transient heat transfer. The experimental results indicated that the pore size of the medium significantly affected the rate of the heat transfer process. A smaller pore size showed a greater effect and could be used in different applications that involve a higher heat transfer rate, while a larger pore size can potentially be used as an insulating material.

Key words: *porous medium, thermal dispersion, thermal radiation, natural-convection, heat transfer enhancement*

Introduction

The transient and steady radiation heat transfer in a porous medium that avoids allowing the passage of fluids has garnered a lot of research interest. It can be used in different applications, such as the petroleum industry, heat recovery, casting of steel, and blood flow [1-3]. Porous media can be used in different applications, such as heat exchangers and electrical equipment. This media can improve the convective heat transfer coefficient and thermal conductivity of the materials by enhancing the contact surface area [4]. Therefore, many studies have extensively focused on the porous materials that are used in different engineering applications, such as chemical contamination of soils and moisture transportation in fibrous insulations [5, 6]. Thermal radiation and thermal dispersion effects also have a high potential weight in nuclear engineering applications, including reactors and propulsion systems. These effects change the temperature distribution in the boundary-layer and on the wall surface when coupled with convection heat flow [7].

The thermal radiation and dispersion effects in the porous medium were studied numerically and analytically investigated in various contexts. In these studies, the natural, mixed

* Corresponding author, e-mail: n.shaban@zuj.edu.jo

and forced convective heat transfer has been numerically investigated. The studies showed a dissipation effect on the isothermal vertical flat plate in the porous medium that was saturated with a fluid [8]. The results indicated that the heat transfer rate was improved with an increase in the Darcy number. It has been noted that the Nusselt number decreased with an increase in the Forchheimer number. In addition, the mixed convection reaction in the side-heated, side-cooled cavity that was filled with the porous medium has been studied [9]. It has been found that the thermal boundary-layer thickness played a vital role in controlling the effect of pore size and grains on the heat transfer rate occurring in the cavity.

The application which gained the most attention involved the presence of the porous medium in the annular cylindrical geometries. In an earlier study, the influence of the opposing flow of the fluid in the vertically aligned porous annulus present in the fluid-saturated porous media has been conducted [10]. This model was numerically solved by using a finite element technique. Other researchers also investigated a similar set-up with different shapes of annulus geometry to enhance the transfer rate [11-18]. A right circular cone with non-Newtonian fluid in saturated porous medium was used to investigate the viscosity, thermal dispersion influences on natural-convection [19]. Mathematical models and experimental works have been carried out to show the influence on heat transfer rate of the porous medium existence in the annular cylindrical-shaped container. This study differs from the other previous studies; because it focuses on the effect of both thermal radiation and dispersion on the isotropic and homogeneous, fluid-saturated porous media, having different particle pore sizes in annular cylinder.

Mathematical formulations

A vertical annular cylinder is filled with saturated porous media. A hot liquid was pumped at a constant temperature in the inner cylinder. As a result, the inner surface of the cylinder had a constant temperature, T_w , and uniform wall thickness. The inner cylinder had a radius of r while the outer cylinder had a radius of r_o . The cylinder height was L . A natural heat transfer takes place in the region filled with saturated porous media. The temperature increased from the inner to the outer cylinder. Figure 1 depicts the environmental temperature.

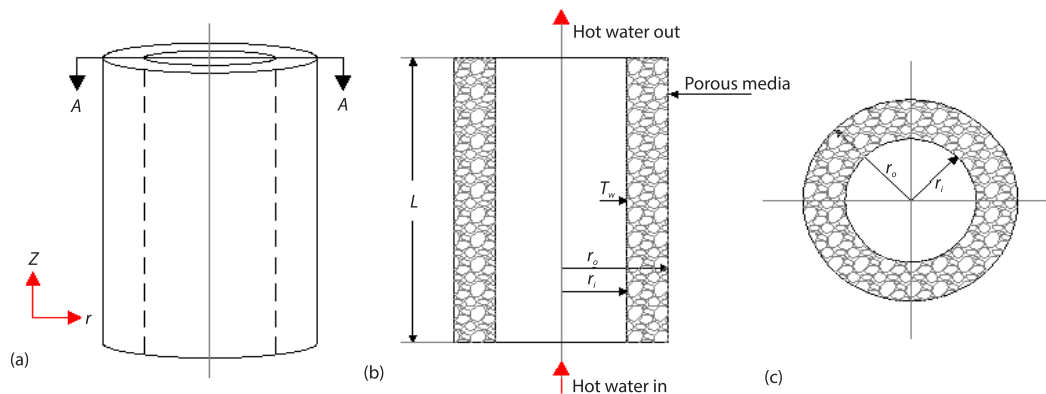


Figure 1. (a) Vertical annular cylinder filled with a saturated porous media, (b) cross-section of the cylinder, A-A, and (c) top view of the cylinder

The used porous medium was isotropic, homogeneous, and saturated with the fluid. The local thermal equilibrium was presumed within the medium and fluid. Furthermore, density (which is a function of temperature) and similar other fluid properties were assumed to be constant.

Governing equations

The governing equations are given by the continuity equation:

$$\frac{\partial}{\partial z}(ru) + \frac{\partial}{\partial u}(rw) = 0 \tag{1}$$

The Darcy-Forchheimer law for flow in porous media.

The *z*-momentum equation:

$$w = \frac{gK}{\nu} \beta_T (T - T_\infty) \tag{2}$$

The *r*-momentum equation:

$$u = \frac{gK}{\nu} \beta_T (T - T_\infty) \tag{3}$$

The energy equation:

$$\frac{\partial T}{\partial t} + u \frac{\partial T}{\partial r} + w \frac{\partial T}{\partial z} = \alpha_e \left[\frac{1}{r} \frac{\partial}{\partial r} \left(r \frac{\partial T}{\partial r} \right) + \frac{\partial^2 T}{\partial z^2} \right] - \frac{1}{\rho c_p} \left[\frac{1}{r} \frac{\partial}{\partial r} (rq_r) + \frac{\partial}{\partial z} (q_z) \right] \tag{4}$$

The density function:

$$\rho = \rho_\infty + [1 - \beta_T (T - T_\infty)] \tag{5}$$

Substituting Rosseland approximation [19] for radiation into the energy equation:

$$q_r = - \frac{4n^2 \sigma}{3\beta_R} \frac{\partial T^4}{\partial r} \tag{6}$$

Where T^4 as a function of T Taylor series [20] is approximately equal to:

$$T^4 \cong 4T_\infty^3 - 3T_\infty^4 \tag{7}$$

$$q_r = - \frac{4n^2 \sigma}{3\beta_R} \frac{\partial}{\partial r} (4TT_\infty^3 - 3T_\infty^4) = - \frac{16n^2 \sigma T_\infty^3}{3\beta_R} \frac{\partial T}{\partial r} \tag{8}$$

The effective thermal diffusivity is divided into two parts. The first one describes the basic thermal diffusivity and the second one covers dispersion thermal diffusivity [21]:

$$\alpha_e = \alpha + \alpha_d \tag{9}$$

$$\alpha_d = \gamma dw \tag{10}$$

$$\alpha = \frac{k}{\rho c_p} \tag{11}$$

Substituting Rosseland approximation and the effective thermal diffusivity. The energy equation becomes:

$$\frac{\partial T}{\partial t} + u \frac{\partial T}{\partial r} + w \frac{\partial T}{\partial z} = \left(\frac{k}{\rho c_p} + \gamma dw \right) \left[\frac{\partial^2 T}{\partial r^2} + \frac{1}{r} \frac{\partial T}{\partial r} + \frac{\partial^2 T}{\partial z^2} \right] - \frac{16n^2 \sigma T_\infty^3}{3\beta_R \rho c_p} \left[\frac{\partial^2 T}{\partial r^2} + \frac{1}{r} \frac{\partial T}{\partial r} + \frac{\partial^2 T}{\partial z \partial r} \right] \tag{12}$$

Initial and boundary conditions

The geometry of annular cylinder is axis symmetric. Initial and boundary conditions:

– At $t = 0$

$$r = r_i \rightarrow T = T_\infty, u = 0 \quad (13a)$$

$$r = r_o \rightarrow T = T_\infty, u = 0 \quad (13b)$$

$$z = 0 \rightarrow T = T_\infty, u = 0 \quad (13c)$$

– At $t > 0$

$$r = r_i \rightarrow T = T_w, u = 0 \quad (14a)$$

$$r = r_o \rightarrow u = 0 \quad (14b)$$

$$z = 0 \rightarrow T = T_\infty \quad (14c)$$

Non-dimensional governing equations

The non-dimensional parameter is defined:

$$U = \frac{u}{u_\infty}, W = \frac{v}{u_\infty}, \theta = \frac{T - T_\infty}{T_w - T_\infty}, t^* = \frac{Ut}{L}, \text{Td} = \frac{d}{L} \quad (15)$$

$$\text{Re} = \frac{UL}{\nu}, \text{Rn} = \frac{4n^2 \sigma T_\infty^3}{\beta_e K}, \text{Gr} = \frac{Lg(T_w - T_\infty)}{U_\infty^2} \quad (16)$$

The dimensionless momentum and energy equations:

– The z -momentum equation

$$W = \text{Gr} \theta \quad (17)$$

– The r -momentum equation

$$U = 0 \quad (18)$$

The energy equation:

$$\frac{\partial \theta}{\partial t^*} = -U \frac{\partial \theta}{\partial R} - W \frac{\partial \theta}{\partial Z} + \left(\frac{1}{\text{Pe}} + \text{Td}W \right) \left[\frac{\partial^2 \theta}{\partial R^2} + \frac{1}{R} \frac{\partial \theta}{\partial R} + \frac{\partial^2 \theta}{\partial Z^2} \right] - \frac{\text{Rn}}{\text{Re}} \left[\frac{\partial^2 \theta}{\partial R^2} + \frac{1}{R} \frac{\partial \theta}{\partial R} + \frac{\partial^2 \theta}{\partial Z \partial R} \right] \quad (19)$$

Non-dimensional Initial and boundary conditions

After applying the non-dimensional parameter eq. (15) into the Initial and boundary conditions eqs. (13) and (14) the dimensionless initial and boundary conditions:

– At $t = 0$

$$R = 1 \rightarrow \theta = 1, U = 0 \quad (20a)$$

$$R = 2 \rightarrow \theta = 1, U = 0 \quad (20b)$$

$$Z = 0 \rightarrow \theta = 1, U = 0 \quad (20c)$$

– At $t > 0$

$$R = 1 \rightarrow \theta = 1, U = 0 \quad (21a)$$

$$R = 2 \rightarrow u = 0 \quad (21b)$$

$$Z = 0 \rightarrow \theta = 0 \quad (21c)$$

Numerical method

Numerical techniques are often used for solving problems that are difficult to solve using analytical methods [22]. A finite-difference technique can be used for solving the quantity, momentum, and energy equations [23]. The implicit methods present a solution by solving the equations that involve the existing and the successive states of the system. A finite-difference approximation is described as the mean properties between the current time step, n , and the subsequent time step ($n + 1$) [24]. Finite difference approximations are substituted into the governing equation by using implicit (Crank-Nicolson) approach:

- The continuity equation

$$U_{ij}^n = 0 \tag{22}$$

- The momentum equation in x -direction

$$W_{ij}^{n+1} = Gr_{j,i}^{\theta n} \tag{23}$$

- The energy equation

$$\begin{aligned} \frac{\theta_{ij}^{n+1} - \theta_{ij}^n}{\Delta t^*} = & (-U_{ij}^n) \left(\frac{\theta_{i+1,j}^n - \theta_{i,j}^n}{\Delta R} \right) - (W_{ij}^n) \left(\frac{\theta_{i,j+1}^{n+1} - \theta_{i,j}^{n+1} + \theta_{i,j+1}^n - \theta_{i,j}^n}{2(\Delta Z)} \right) + \left(\frac{1}{Pe} + Td W_{i,j}^n \right) \cdot \\ & \cdot \left[\frac{\theta_{i+1,j}^n - 2\theta_{i,j}^n + \theta_{i-1,j}^n}{\Delta R^2} + \frac{1}{R} \left(\frac{\theta_{i+1,j}^n - \theta_{i-1,j}^n}{\Delta R} \right) \dots + \frac{\theta_{i,j+1}^{n+1} - 2\theta_{i,j}^{n+1} + \theta_{i,j-1}^{n+1} + \theta_{i,j+1}^n - 2\theta_{i,j}^n + \theta_{i,j-1}^n}{2(\Delta Z)^2} \right] - \\ & - \frac{Rn}{Re} \left[\frac{\theta_{i+1,j}^n - 2\theta_{i,j}^n + \theta_{i-1,j}^n}{\Delta R^2} + \frac{1}{R} \left(\frac{\theta_{i+1,j}^n - \theta_{i-1,j}^n}{\Delta R} \right) + \frac{\theta_{i,j+1}^{n+1} - \theta_{i,j}^{n+1} + \theta_{i,j+1}^n - \theta_{i,j}^n}{2(\Delta Z)(\Delta R)} \right] \end{aligned} \tag{24}$$

Substituting the finite difference approximation into the energy equation, yields:

$$A\theta_{i,j+1}^{n+1} + B\theta_{i,j}^{n+1} + C\theta_{i,j-1}^{n+1} = D \tag{25}$$

where the coefficient A , B , C , and D are given:

$$A = \left[\frac{W_{ij}^n}{2(\Delta Z)} \right] - \frac{1}{2(\Delta Z)^2} \left(\frac{1}{Pe} + Td W_{ij}^n \right) + \frac{Rn}{2Re(\Delta Z)(\Delta R)} \tag{26}$$

$$B = \frac{1}{\Delta t^*} - \frac{W_{i,j}^n}{2(\Delta Z)} + \frac{1}{(\Delta Z)^2} \left(\frac{1}{Pe} + Td W_{i,j}^n \right) - \left[\frac{Rn}{2Re(\Delta Z)(\Delta R)} \right] \tag{27}$$

$$C = \frac{-1}{2(\Delta Z)^2} \left(\frac{1}{Pe} + Td W_{i,j}^n \right) \tag{28}$$

$$\begin{aligned} D = & \frac{\theta_{i,j}^n}{\Delta t^*} + (-U_{ij}^n) \left(\frac{\theta_{i+1,j}^n - \theta_{i,j}^n}{\Delta R} \right) + (-W_{ij}^n) \left(\frac{\theta_{i,j+1}^n - \theta_{i,j}^n}{2(\Delta Z)} \right) + \\ & + \left(\frac{1}{Pe} + Td W_{ij}^n \right) \left(\frac{\theta_{i+1,j}^n - 2\theta_{i,j}^n + \theta_{i-1,j}^n}{\Delta R^2} + \frac{1}{R} \left(\frac{\theta_{i+1,j}^n - \theta_{i-1,j}^n}{\Delta R} \right) + \frac{\theta_{i,j+1}^n - 2\theta_{i,j}^n + \theta_{i,j-1}^n}{2(\Delta Z)^2} \right) - \\ & - \frac{Rn}{Re} \left(\frac{\theta_{i+1,j}^n - 2\theta_{i,j}^n + \theta_{i-1,j}^n}{\Delta R^2} + \frac{1}{R} \left(\frac{\theta_{i+1,j}^n - \theta_{i-1,j}^n}{\Delta R} \right) + \frac{\theta_{i,j+1}^n - \theta_{i,j}^n}{2(\Delta Z)(\Delta R)} \right) \end{aligned} \tag{29}$$

The local Nusselt number:

$$\text{Nu} = \left[\frac{\theta_{j,i}^n - \theta_{j-1,i}^n}{Z} \right]_{y=0} \quad (30)$$

The systems of equation are solved by using commercial software MALAB. The results are presented in section *Results and discussion*.

Experimental data

Experimental set-up

In this study, the researchers designed a heat exchanger, which had an annular vertical cylindrical shape. The inner cylinder showed an inner and outer diameter of 40 cm and 60 cm, respectively. The two cylinders were 120 cm high. This heat exchanger was further raised from the ground by 20 cm with the help of four steel pillars for avoiding heat dissipation that could occur from the exchanger to the floor by conduction. The region between the inner and outer cylinders was filled using three types of porous media, with three differing grain sizes, *i.e.*, coarse, medium, and fine. For determining the temperature distribution within the porous media, the researchers evenly distributed six *K*-type thermocouples in the region between both the cylinders as shown in fig. 2. All these thermocouples were connected to the data logger (HiokiLR8431), which recorded the temperature values during experimentation with a resolution of 0.1 °C.

The inner cylinder contained an electrical heating element (2 kW) that was connected to the power supply present outside the complete set-up. A heater was used for generating thermal energy within the heat exchanger. Thereafter, this inner cylinder was filled with water, as shown in fig. 2. Then, this inner cylinder was sealed shut from both the top and the bottom ends for preventing the entry of air into the system. Water inlet and outlet units were installed at the top and the bottom ends of the inner cylinder, respectively. Finally, an electrical water pump was installed outside for circulating the water, through the heat exchanger which was connected to the inner cylindrical unit. This pump generated a steady flow in the heat exchanger as it removed the hot water collected at the bottom outlet of the inner cylinder and pumped it back to the inlet of the cylinder, as shown in fig. 2.

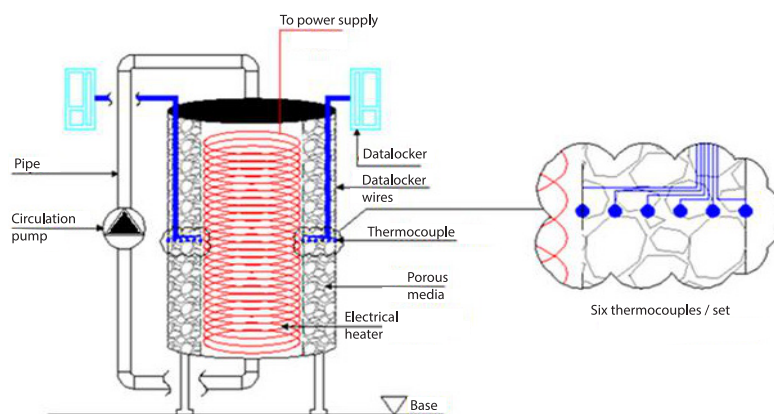


Figure 2. Lay-out of the experimental set-up

Three experiments were conducted using the previous set-up. Before initiating any experiment initially, the researchers filled the region between the inner and the outer cylinders

Table 1. Prosperities of porous media used

Abbreviation	(a)	(b)	(c)
Type	Fine	Medium	Course
Average grain size [mm]	1	9	34
Solid density [Kgm ⁻³]	2210	2210	2210
Solid heat capacity [JKg ⁻¹ K ⁻¹]	840	840	840
Solid thermal conductivity [Wm ⁻¹ K ⁻¹]	2.15	2.15	2.15

were filled with a specific porous medium according to the tab. 1. The top of the heat exchanger was closed using a steel lid, as shown in fig. 3. Then, the electrical heater and water pump were turned on, which enabled the data logger to start recording the temperature values using the thermocouples. The duration of every experiment was 60 minutes. All the aforementioned experiments were carried out in the heat transfer laboratory at the Al Zaytoonah University, Jordan, in November, 2020.



Figure 3. Test device used in the experimental study

Experimental results

Table 2 shows the temperatures of porous media at different radius for different types of porous media are shown in tab. 2. Figure 5 shows the temperature distribution profile for the three kinds of porous media described in tab. 1 and fig. 4 for differing time periods. The maximum temperature was defined as the temperature value of the inner vertical plane, wherein an equal volume of water passed the inner pipe and was constant for the different periods. The temperatures of the saturated liquid passing through the thermal boundary-layer increased gradually during the transient period, till it reaches a steady-state. In the steady-state, the temperature of the fluid in the thermal boundary-layer was equivalent to the temperature of the saturated fluid existing outside the boundary-layer. At a specified period, the experimental results indicated that the temperature of the saturated fluid in the thermal boundary-layer for Type (a) was higher than the temperature value for the saturated fluid for Type (b). Furthermore, the temperature of the saturated fluid in the thermal boundary-layer for Type (b) was higher than the temperature of the saturated fluid for Type (c). Thus, the small pore diameters of the media particles increased the thickness of the thermal boundary-layer through the transient and steady periods.

Table 2. Measured temperature [°C] for different samples at different time periods

Radius [mm]	Type (a)			Type (b)			Type (c)		
	5 minutes	20 minutes	60 minutes	5 minutes	20 minutes	60 minutes	5 minutes	20 minutes	60 minutes
20	80	80	80	80	80	80	80	80	80
22	26	30.5	50.2	32	40.5	55.4	35.8	49.5	60.6
24	22	25.5	40.3	24.6	30.4	45.6	27.6	33	49.4
26	22.1	22.6	31	22.8	24.6	33.9	24.5	27.2	40.6
28	22.1	22.3	27.2	22.7	22.5	28.7	22.6	23.2	32.4
30	22	22.4	25.5	22	22	26	22.6	22	27.5



Figure 4. Different types of porous media used in the study

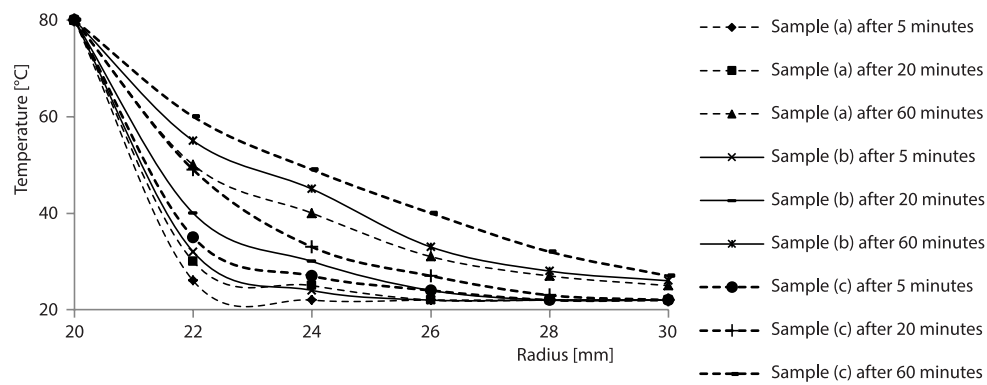


Figure 5. Experimental temperature profile for the three kinds of porous media considered for different periods

Results and discussion

Thermal radiation effect

The thermal radiation effect on the Darcy natural-convection cycles passing through the annular vertical cylinders that are filled with the liquid and saturated porous media is shown in both figs. 6 and 7. The velocity and temperature profiles for the various thermal radiation cycles for different Rn and time period are presented. As described in fig. 6 the edges of the cylinder show a zero velocity while it is a maximum at the centre. As the time passes, the momentum boundary-layer gradually increased and became a maximum at the centre of the cylinder.

At any specified time period, the momentum layer due to thermal radiation was larger than that arising without any thermal radiation. Similarly, the thermal layer that was formed due to thermal radiation was larger than that arising without any thermal radiation. Figure 8 shows the local Nusselt number of porous media for the various radiation values. The results indicated that at any specified thermal dispersion value, the local Nusselt number decreased through the transient time. At any time period, the values of the local Nusselt number arising due to the higher thermal radiation were smaller compared to the Nusselt numbers arising due to a lower thermal radiation.

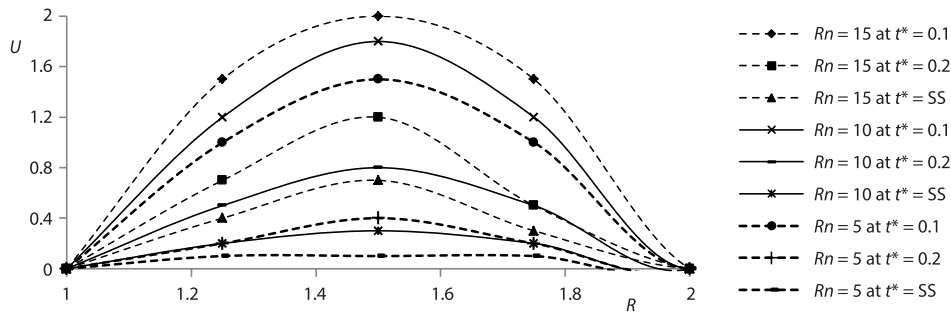


Figure 6. Dimensionless velocity profiles for different thermal radiation values

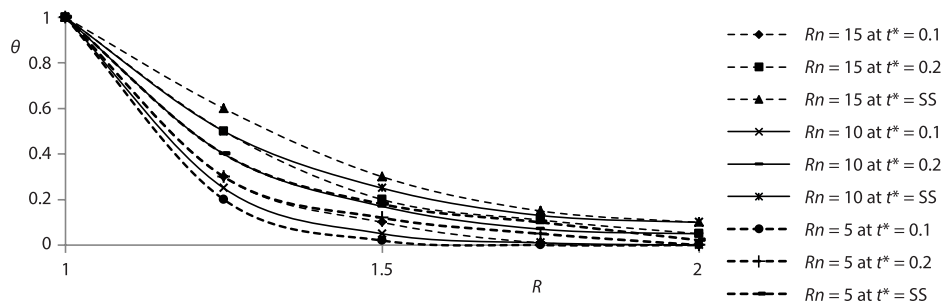


Figure 7. Dimensionless temperature profiles for different radiation values

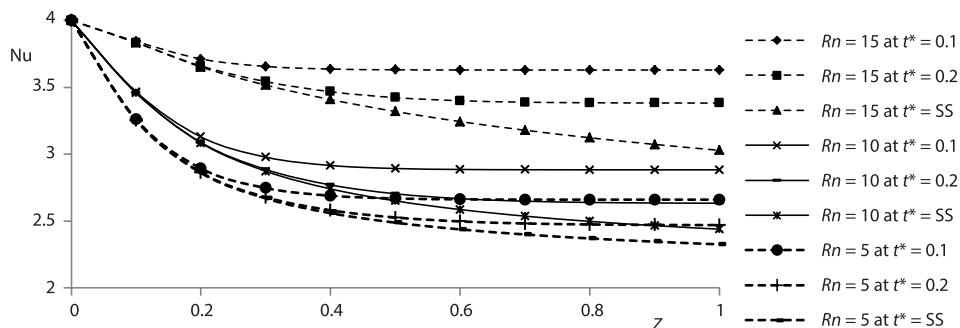


Figure 8. Local Nusselt number for different dimensionless height values

Thermal dispersion effect

Thermal dispersion number describes the mechanical dispersion of porous media which is directly affected by conduction and convection heat transfer. The experimental results indicated that the thermal dispersion affected the Darcy natural-convection cycles occurring in the annular vertical cylinders used in the study. As mentioned previously, these cylinders were filled with three different kinds of saturated porous fluid media, having different grain sizes. The lowest grain size of porous media of the most decreasing in temperature is chosen to show thermal depression effect when the numerical solution is developed. Figures 9 and 10 depict the velocity and temperature profiles noted after experimentation when different thermal dispersion cases were used. As presented in fig. 9 the velocity at the edge of the inner cylinder was zero, while it was a maximum at the centre of the cylinder. When the thermal dispersion cycle was

carried out for different time periods, the results indicated that the thickness of the momentum boundary-layer increased gradually and was found to be a maximum at the centre of the inner cylinder. At any particular time period, the thickness of the momentum boundary-layer due to the presence of thermal dispersion was lower than that noted in the absence of any thermal dispersion. Furthermore, the thermal layer formed because of thermal dispersion was lower than that noted in the absence of thermal dispersion.

Figure 11 depicts the local Nusselt number for the different porous media sizes and different thermal dispersion values. The experimental results showed that at a specific thermal dispersion value, the local Nusselt number gradually decreased over a transient time period. At a specified period, the local Nusselt number noted in the presence of a higher thermal dispersion value is smaller than the Nusselt number noted in case of low thermal dispersion.

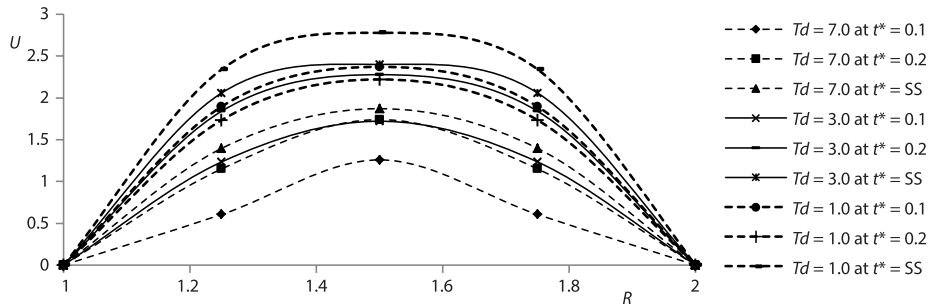


Figure 9. Dimensionless velocity profiles for the porous media particles for the different thermal dispersion numbers

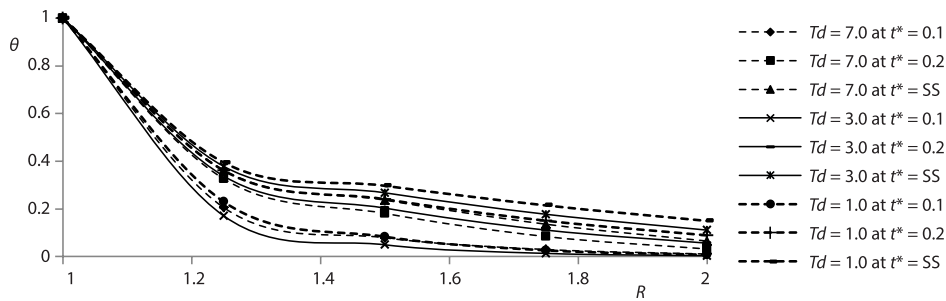


Figure 10. Dimensionless temperature profiles for the porous media particles for the different thermal dispersion numbers

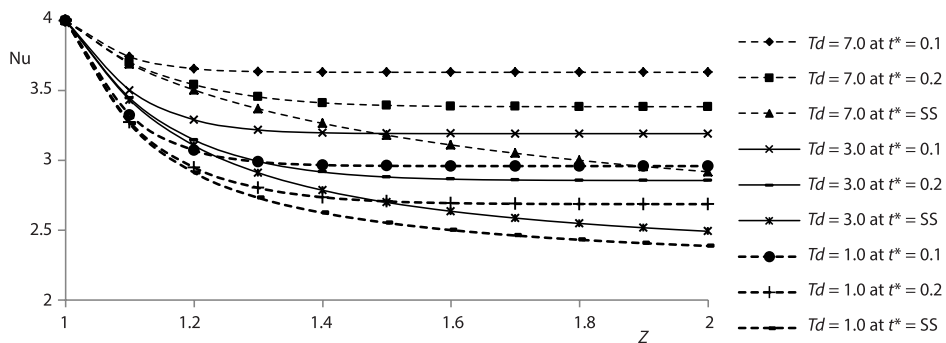


Figure 11. Local Nusselt number for the porous media when different thermal dispersion numbers were used in the experiment

Validation

Validation of the experimental part

A numerical model was developed using ANSYS 18.2 and validated with the experimental results to provide more information of the heat transfer in porous media. The validation was carried out using steady-state condition for the three samples. Figure 12 shows the validation of the numerical results against the experimental results. It was shown that the numerical results are in a good agreement with the experimental results. In addition, fig. 13 shows the temperature contours through the porous media for the three samples.

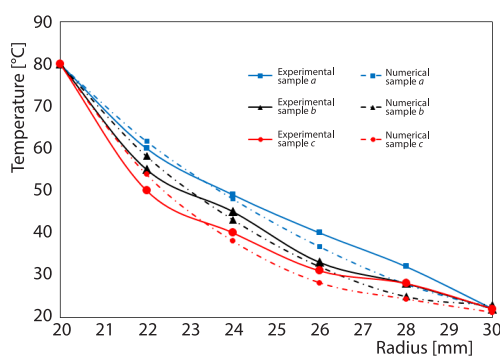


Figure 12. Numerical validation against the experimental results for the three samples

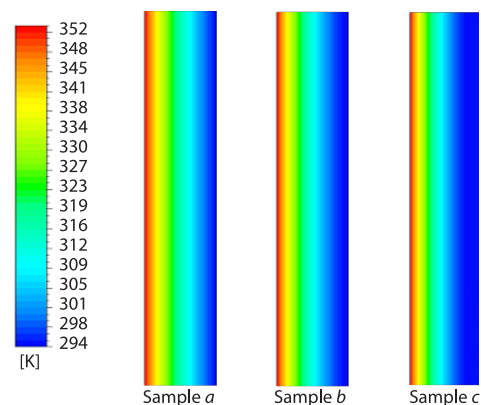


Figure 13. Temperature contours for the three samples

Validation of the numerical solution part

Intensive searches in much previous literature are done by the authors to find any similar work to validate the present numerical solution. It is found that the previous studies have just focused on either the thermal radiation or the effect thermal depression but not both. Figure 4 in reference [25] shows that about 66% increasing in the local Nusselt number when Radiation number is increased from 0 to 1, which agrees with this study as shown in fig. 8.

Moreover, figures [11-13], in [8] show increasing in velocity, temperature, and local Nusselt number when thermal dispersion numbers are increased. These results agree with this work as shown in figures [9-11].

Conclusions

In this study, the effect of thermal radiation and dispersion in an annular vertical cylinder filled with porous media has been investigated. The experiments were conducted over natural-convection heat transfer cycles. These effects were determined using some parameters involving the dimensionless group such as velocity, U , temperature, θ , and the local Nusselt number, Nu . Additionally, momentum, continuity, energy equations and boundary conditions that can be converted to the dimensionless equations were numerically solved using the finite difference Crank-Nicolson method. Further, the effects of the pore size of the porous media particles using different kinds of media were experimentally determined and numerical model was developed to validate the experimental work. Pore sizes of porous media could be determined to maximize or minimize heat transfer rate. The results obtained by the numerical ANSYS model were in good agreement with experimental results, also the validation of numerical solution agrees with the existing of the previous literature.

It was noted that when there was an increase or a decrease in the thermal dispersion factor, the thickness of the momentum boundary-layer is increased. The thickness of the thermal boundary-layer also increased in the natural-convection heat transfer process. However, in the case of a natural-convection heat transfer, the temperature and velocity of the saturated fluid through the thermal and momentum boundary-layer is increased gradually during the transient time till it reached a steady-state. The dispersion parameter, γ , that increased the thermal dispersion, also increased the momentum and the thickness of the thermal boundary-layer through steady and transient time periods. Moreover, during a natural-convection heat transfer process, when the pore size of the porous media increased, the thickness of the thermal boundary-layer decreased through transient time. After determining pore sizes and both profiles of temperature and velocity according to the effect of Radiation number and R_d , the rate of heat transfer could be known regarding the specified thermal processes required.

Acknowledgment

This research was financially supported by Al-Zaytoonah University of Jordan under Grant No.17/12/2019-2020.

Nomenclature

c_p – specific heat, [$\text{JKg}^{-1}\text{K}^{-1}$]
 d – pore diameter, [m]
 g – gravitational acceleration, [ms^{-2}]
 h – convection heat transfer coefficient, [$\text{Wm}^{-2}\text{K}^{-1}$]
 K – permeability, [m^{-1}]
 L – length of vertical plate, [m]
 Nu – local Nusselt number
 n – refractive index
 Pe – Peclet number
 q_r – radiation flux, [Wm^{-2}]
 R – dimensionless radius
 Re – Reynolds number
 Rn – radiation number
 r – radius, [m]
 T – temperature, [K]
 Td – thermal dispersion effect number
 t – time, [s]
 t^* – dimensionless time
 U – dimensionless velocity in X -direction.
 u – velocity in r -directions, [ms^{-1}]
 W – dimensionless velocity in R -direction

w – velocity in z -directions, [ms^{-1}]
 Z – dimensionless height
 z – neight, [m]

Greek symbols

α – molecular thermal diffusivity, [m^2s^{-1}]
 α_d – dispersion thermal diffusivity, [m^2s^{-1}]
 β_R – rosseland extinction coefficient
 β_r – coefficient of thermal expansion
 γ – coefficient of mechanical dispersion
 θ – dimensionless temperature
 ν – kinematic viscosity, [m^2s^{-1}]
 σ – Stefan-Boltzmann constant, [$\text{Wm}^{-2}\text{K}^{-4}$]

Subscripts

i – index for point $P(i, j)$ in the r -direction
 j – index for point $P(i, j)$ in the z -direction
 w – surface conditions
 ∞ – free stream condition

Acronym

SS – steady-state

References

- [1] Alibakhsh, A., *et al.*, Nanofluid-flow and Heat Transfer in Porous Media: A Review of the Latest Development, *International Journal of Heat and Mass Transfer*, 107 (2017), Apr., pp. 778-791
- [2] Kandelousi, M., *et al.*, *Nanofluid-flow in Porous Media: BoD–Books on Demand*, 2020
- [3] El-Dabe, N., *et al.*, The Motion of a non-Newtonian Nanofluid over a Semi-Infinite Moving Vertical Plate through Porous Medium with Heat and Mass Transfer, *Thermal Science* 24 (2020), 2B, pp. 1311-1321
- [4] Mahian, O., *et al.*, Recent Advances in Modelling and Simulation of Nanofluid-Flows-Part I: Fundamentals and Theory, *Physics Reports*, 790 (2019), Feb., pp. 1-48
- [5] Badruddin, I., *et al.*, Analysis of Heat and Mass Transfer in a Vertical Annular Porous Cylinder Using FEM, *Transport in Porous Media*, 91 (2012), 2, pp. 697-715

- [6] Abdel Hafez, E., et al., Effect of an Insulation Layer to Prevent Water Vapor Condensation Along the Inside Surface of a Building Wall Using an Artificial Neural Network: *Journal of Infrastructure Systems*, 22 (2014), Jan., pp. A4014005-1-A4014005-7
- [7] Abdul Gaffar, S., et al., Thermal Radiation and Heat Generation/Absorption Effects on Viscoelastic Double-Diffusive Convection from an Isothermal Sphere in Porous Media, *Ain Shams Engineering Journal*, 6 (2021) 3, pp. 1009-1030
- [8] Nasser, I., Duwairi, H. M., Thermal Dispersion Effects on Convection Heat Transfer in Porous Media with Viscous Dissipation, *International Journal of Heat and Technology*, 34 (2016), 2, pp. 207-212
- [9] Chakkingal, M., et al., Assisting and Opposing Mixed Convection with Conjugate Heat Transfer in a Differentially Heated Cavity Filled with Coarse-Grained Porous Media, *International Communications in Heat and Mass Transfer*, 111 (2020), 104457
- [10] Al-Rashed, A., et al., Mixed Convection Opposing Flow in a Vertical Porous Annulus-Two Temperature Model, IOP Conference Series, *Materials Science and Engineering*, 149 (2016), 012214
- [11] Baig, A., et al., Discrete Heating of Opposing Mixed Convection Heated at Bottom of Annulus, *Proceedings*, 1st International Conference on Manufacturing, Material Science and Engineering, (Icmmse-2019), Kandlakoya, India, 19, AIP Publishing,
- [12] Pushpa, B. V., et al., Optimization of Thermosolutal Convection in Vertical Porous Annulus with a Circular Baffle, *Thermal Science and Engineering Progress*, 20 (2020), 100735
- [13] Hamza, M., et al., Mixed Convection Flow of Viscous Reactive Fluids with Thermal Diffusion and Radial Magnetic Field in a Vertical Porous Annulus, *Computational Mathematics and Modelling*, 30 (2019), 3, pp. 239-253
- [14] Badruddin, I., et al., Conjugate Heat and Mass Transfer in a Vertical Porous Cylinder, *Journal of Thermophysics and Heat Transfer*, 33 (2019), 2, pp. 548-558
- [15] Miles, A., et al., Heat Transfer and Entropy Generation Analysis of 3-D Nanofluids Flow in a Cylindrical Annulus Filled with Porous Media, *International Communications in Heat and Mass Transfer*, 124 (2021), 105240
- [16] Kilic, M., A Heat Transfer Analysis from a Porous Plate with Transpiration Cooling, *Thermal Science*, 23 (2019), 5B, pp. 3025-3034
- [17] Elbashbeshy, E., et al., Effects of Thermal Radiation and Heat Transfer over an Unsteady Stretching Surface Embedded in a Porous Medium in the Presence of Heat Source or Sink, *Thermal Science*, 15 (2011), 2, pp. 477-485
- [18] Rashed, Z., et al., Heat Transfer Enhancement in the Complex Geometries Filled with Porous Media, *Thermal Science*, 25 (2021), 1A, pp. 39-57
- [19] Kairi, R. R., Viscosity and Dispersion Effects on Natural-Convection from Vertical Cone in a non-Newtonian-Fluid Saturated Porous Medium, *Thermal Science*, 15 (2011), Suppl. 2, pp. S307-S316
- [20] Yih, K. A., Radiation Effect on Natural-Convection over a Vertical Cylinder Embedded in Porous Media, *International Communications in Heat and Mass Transfer*, 26 (1999), 2, pp. 259-267
- [21] Raptis, A., Radiation and Free Convection Flow through a Porous Medium, *International Communications in Heat and Mass Transfer*, 25 (1998), 2, pp. 289-295
- [22] Plumb, O. A., The Effect of Thermal Dispersion on Heat Transfer in Packed Bed Boundary-Layers, *Proceedings*, ASME/JSME Thermal Engineering Joint Conference, Honolulu, Hi., USA, 1983, Vol. 2, pp 17-21
- [23] Muratova, G., et al., Numerical Solution of the Navier–Stokes Equations Using Multigrid Methods with HSS-Based and STS-Based Smoothers: *Symmetry*, 122 (2020), 233
- [24] Khader, M., et al., Numerical Simulation Using the Finite Difference Method for the Flow and Heat Transfer in a Thin Liquid Film over an Unsteady Stretching Sheet in a Saturated Porous Medium in the Presence of Thermal Radiation, *Journal of King Saud University-Engineering Sciences*, 251 (2013), 1, pp. 29-34
- [25] Badruddin, I., et al., Heat Transfer by Radiation and Natural-Convection through a Vertical Annulus Embedded in Porous Medium, *International Communications in Heat and Mass Transfer*, 33 (2006), 4, pp. 500-507